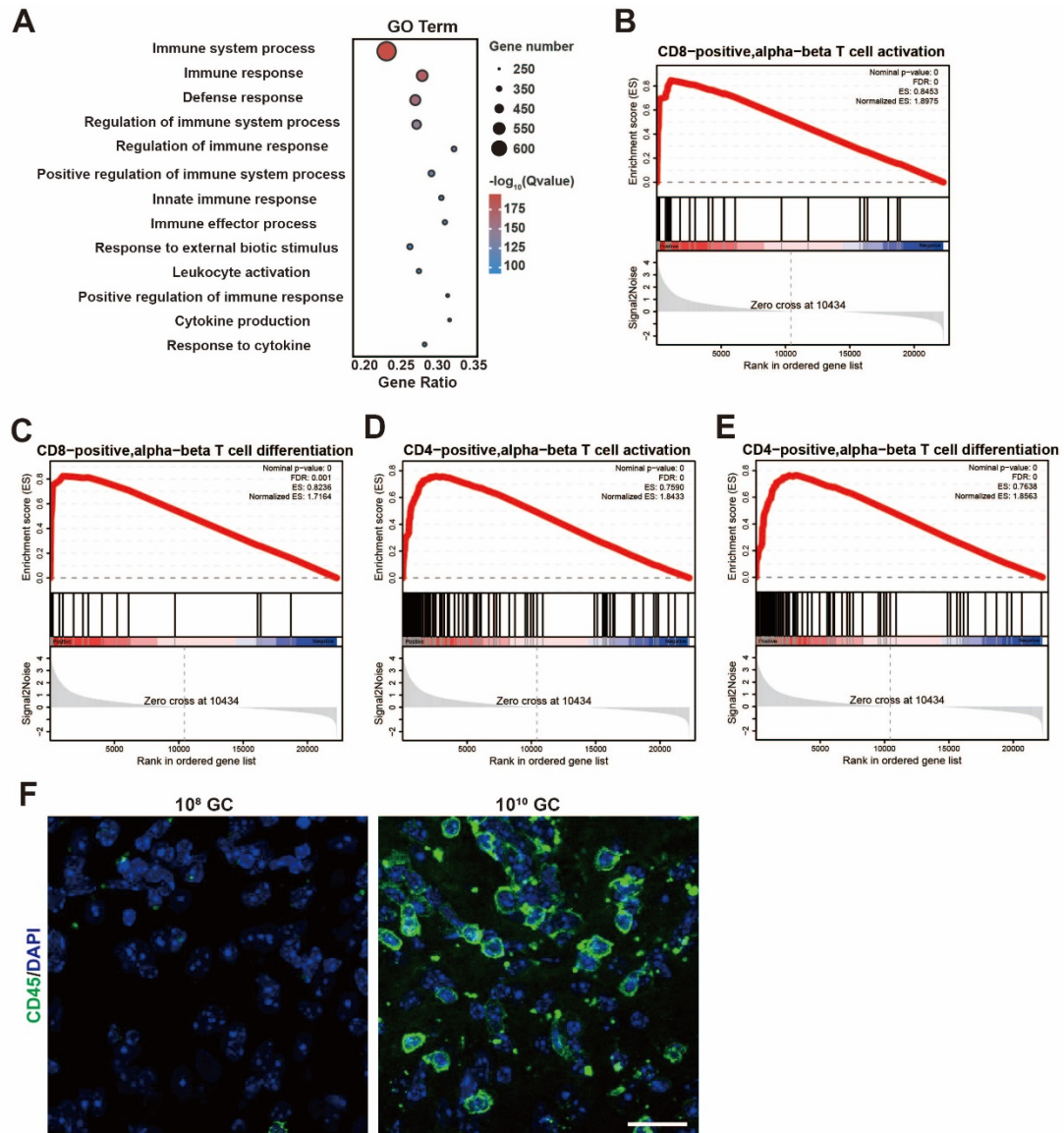


**OMTM, Volume 31**

**Supplemental information**

**High-titer AAV disrupts cerebrovascular  
integrity and induces lymphocyte  
infiltration in adult mouse brain**

**Yaowei Guo, Junliang Chen, Wenyu Ji, Liang Xu, Yu Xie, Shu He, Chuying Lai, Kaiyu Hou, Zeru Li, Gong Chen, and Zheng Wu**



**Figure S1. The GO term and GSEA (Gene Set Enrichment Analysis) analysis of bulk RNA-seq.** (A) Go-enriched bubble plots showing that high doses of virus induce strong immune responses in mouse brains. (B) GSEA analysis of CD8-positive alpha-beta T cell activation. (C) GSEA analysis of CD8-positive alpha-beta T cell differentiation. (D) GSEA analysis of CD4-positive alpha-beta T cell activation. (E) GSEA analysis of CD4-positive alpha-beta T cell differentiation. (F) Confocal imaging of CD45 (green, leukocyte marker) at 30 dpi. Note that many CD45<sup>+</sup> leukocytes were detected in the brain parenchyma after high-titer AAV injection. Scale bar = 20 μm.

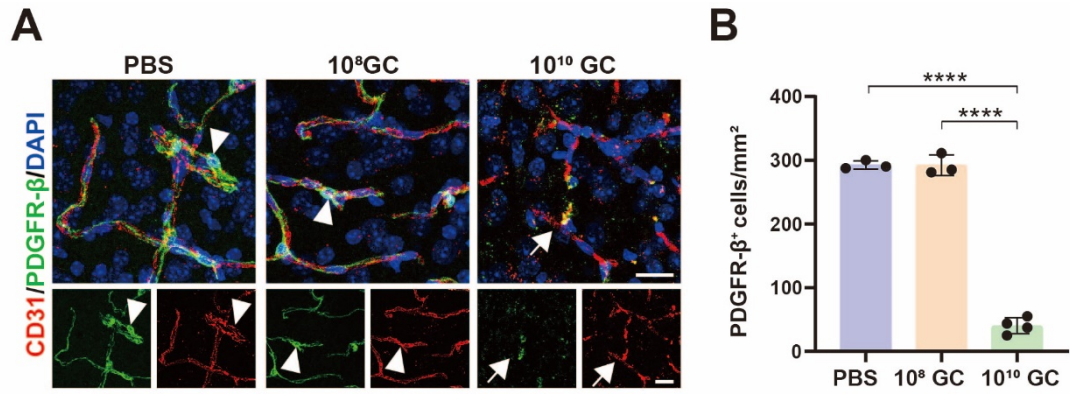


**Figure S2. High-titer AAVs result in pericyte injury.** (A) Confocal imaging of CD31 (red, endothelial cell marker) co-stained with PDGFR- $\beta$  (green, pericyte marker) at 30 dpi. In PBS and 10<sup>8</sup> GC groups, many pericytes were associated with endothelial cells (CD31<sup>+</sup>, indicated by arrowheads), however, pericytes were significantly damaged and endothelial cells lost pericyte sheath (indicated by arrows) in 10<sup>10</sup> GC group. Scale bar = 20  $\mu$ m. (B) Quantifications of PDGFR- $\beta$ <sup>+</sup> cell numbers in PBS, 10<sup>8</sup> GC and 10<sup>10</sup> GC groups. Values are shown as mean  $\pm$  SD. n = 3-4 mice per group. One-way ANOVA analysis with Tukey test. Significance reported as \*\*\*\*p < 0.0001.

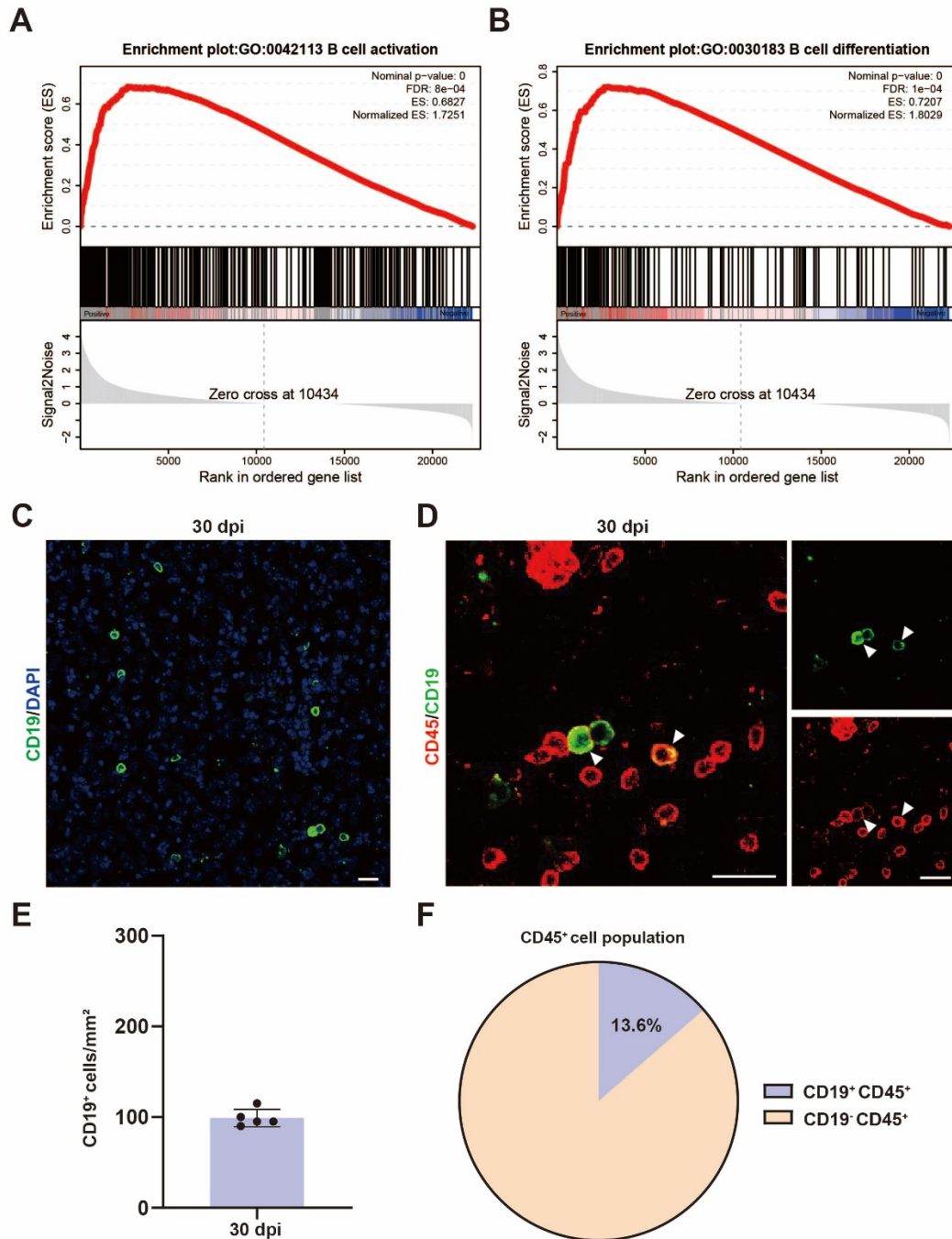


**Figure S3. High-titer AAVs cause B cell infiltration.** (A, B) GSEA analysis of B cell activation (A) and differentiation (B). (C) CD19 immunostaining (B cell marker) in the cortex at 30 days post high-titer AAV injection. Scale bar = 20  $\mu\text{m}$ . (D) Confocal imaging of CD45 (red) co-stained with CD19 (green) at 30 dpi. CD19-positive cells were well co-labeled with CD45 (indicated by arrowheads). Scale bar = 20  $\mu\text{m}$ . (E) Quantification of CD19<sup>+</sup> cell numbers at 30 dpi. (F) The pie chart showing that 13.6% of CD45<sup>+</sup> cells are CD19 positive.

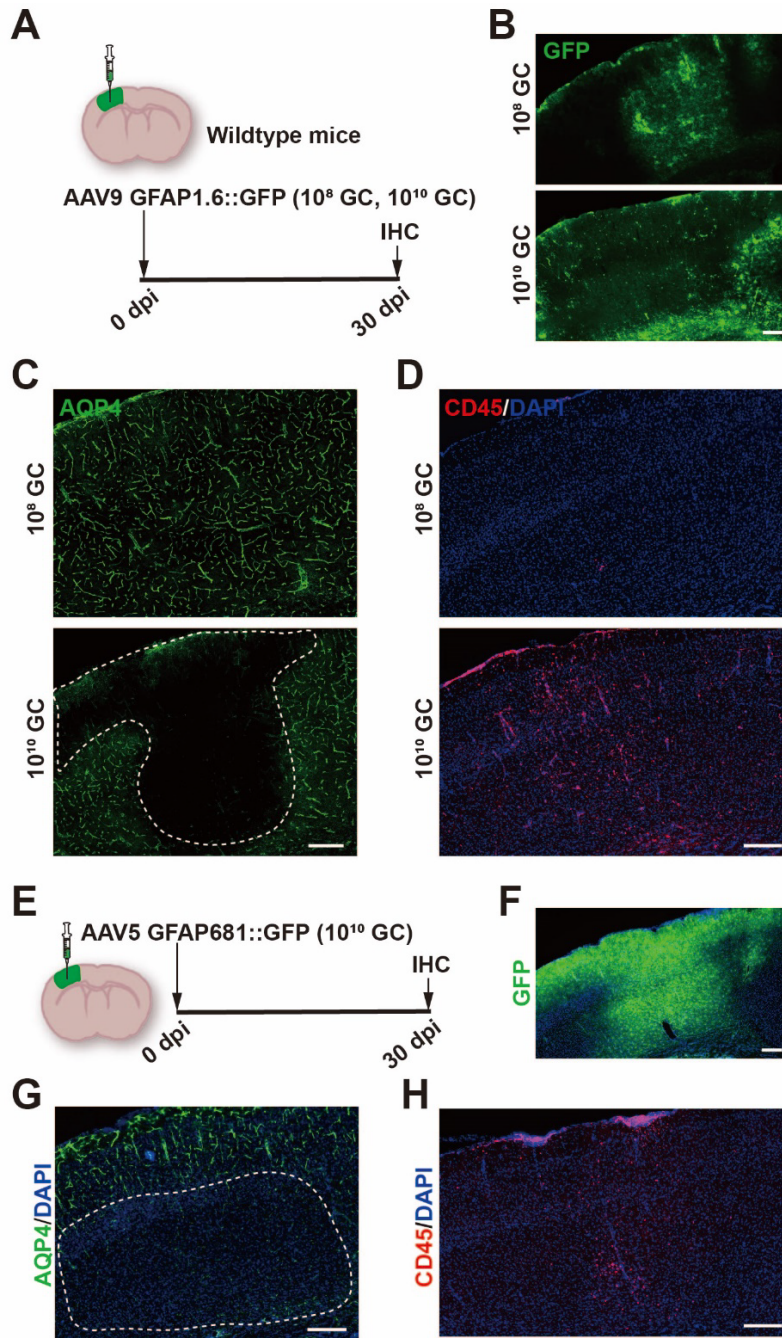


**Figure S4. Different subtypes of GFAP promoters also cause immune cell infiltration.** (A) Experimental design of GFAP1.6 promoter. (B) GFP expression in  $10^8$  GC and  $10^{10}$  GC groups at 30 dpi. Scale bar = 200  $\mu$ m. (C) AQP4 (green) signals were lost in high-titer AAV9 injected area (bottom, white dashed box) compare to low-titer AAV9 treated mice (top). Scale bar = 200  $\mu$ m. (D) CD45 positive immune cells infiltrated the cortex of mice in  $10^{10}$  GC group. Scale bar = 200  $\mu$ m. (E) Experimental design of GFAP681 promoter. (F) GFP expression in  $10^{10}$  GC group at 30 dpi. Scale bar = 200  $\mu$ m. (G) AQP4 (green) signals were lost in the area of injecting with  $10^{10}$  GC AAV5 (white dashed box). Scale bar = 200  $\mu$ m. (H) The mouse cortex was infiltrated by CD45-positive cells in  $10^{10}$  GC group. Scale bar = 200  $\mu$ m.

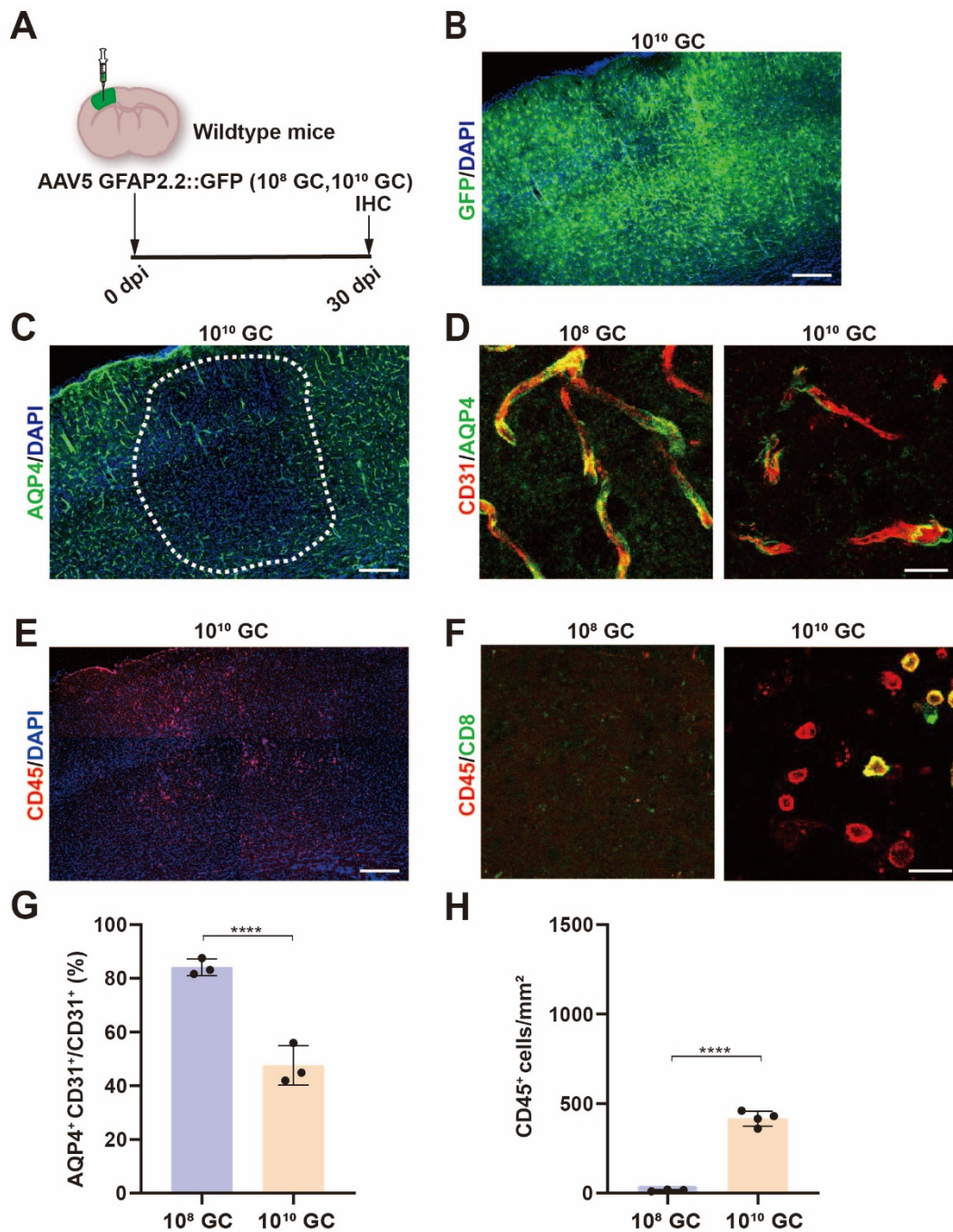


**Figure S5. High-titer AAV5 also results in BBB disruption and leukocyte infiltration.** (A) Experimental design of AAV5 intracranial injection study. (B) GFP expression in the cortex at 30 dpi. Scale bar = 200  $\mu$ m. (C) AQP4 signals were lost in the high-titer AAV5 infected brain regions (white dashed box). Scale bar = 200  $\mu$ m. (D) High-magnification images of CD31 (red) co-stained with AQP4 (green) in low-titer (left) and high-titer AAV5 (right) treated mice at 30 dpi. Scale bar = 20  $\mu$ m. (E) Low-magnification images of CD45 immunostaining (red) in high-titer AAV5 treated mouse brain at 30 dpi. Scale bar = 200  $\mu$ m. (F) High-magnification images of CD45 (red) co-stained with CD8 (green) in low-titer (left) and high-titer AAV5 (right) treated mice at 30 dpi. Scale bar = 20  $\mu$ m. (G) Quantified data showing the ratio of total AQP4<sup>+</sup> signals

to total CD31<sup>+</sup> signals at 30 dpi. (H) Quantifications of CD45<sup>+</sup> cell density at 30 dpi. Values are shown as mean ± SD. n = 3-4 mice per group. Two-tailed Student's t-test. Significance reported as \*\*\*\*p < 0.0001.

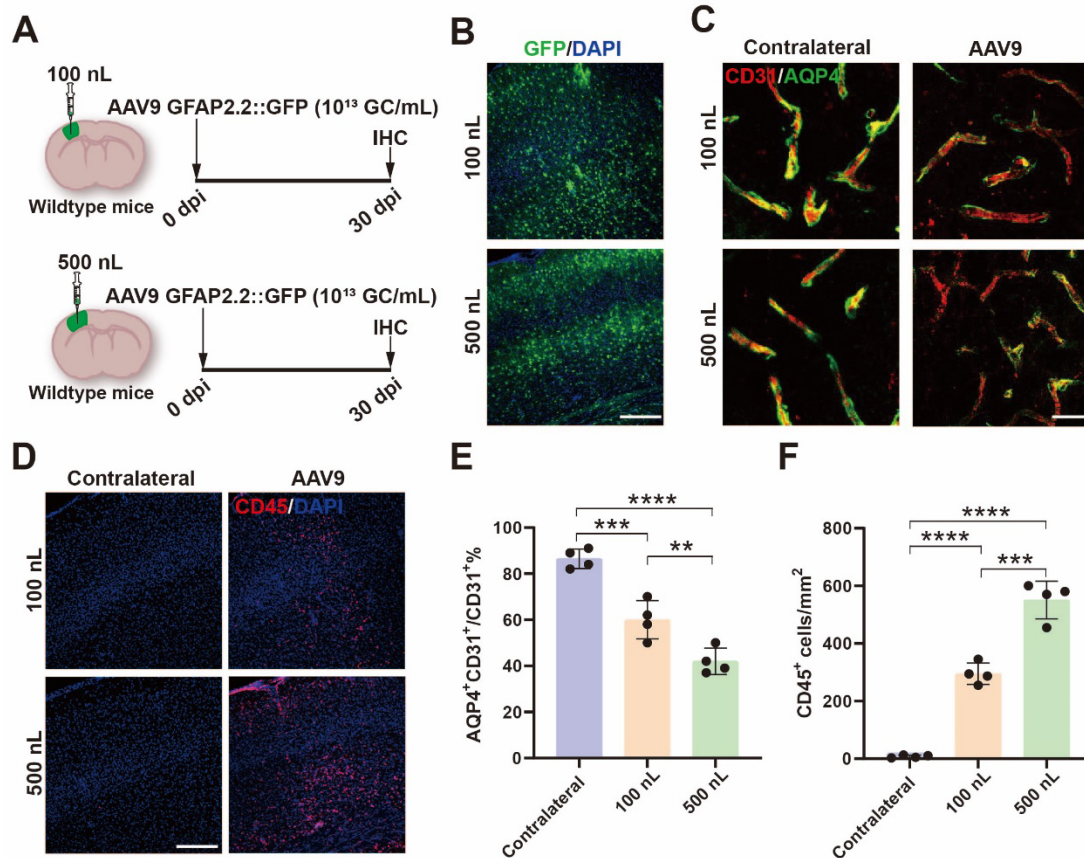


**Figure S6. High-titer AAVs cause BBB disruption and leukocyte infiltration under injection volume below 1  $\mu$ L conditions.** (A) AAV injected area, volume, serotype and experimental timeline. (B) GFP expression in the cortex after injection of 100 nL (top) and 500 nL (bottom) AAV9. Scale bar = 200  $\mu$ m. (C) Decreased AQP4 was detected perivascularly in both 100 nL and 500 nL injected mice compared to the contralateral side. Scale bar = 20  $\mu$ m. (D) Leukocyte infiltration was also presented in both 100 nL and 500 nL injected areas. Scale bar = 200  $\mu$ m. (E) Quantified data showing the percentage of cerebral blood vessels with AQP4 sheath at 30 dpi. (F) Quantifications of CD45<sup>+</sup> cell density at 30 dpi. Values are shown as mean ± SD. n = 4 mice per group. One-way ANOVA analysis with Tukey test. Significance reported as \*\*p < 0.01, \*\*\*p < 0.001. \*\*\*\*p < 0.0001.

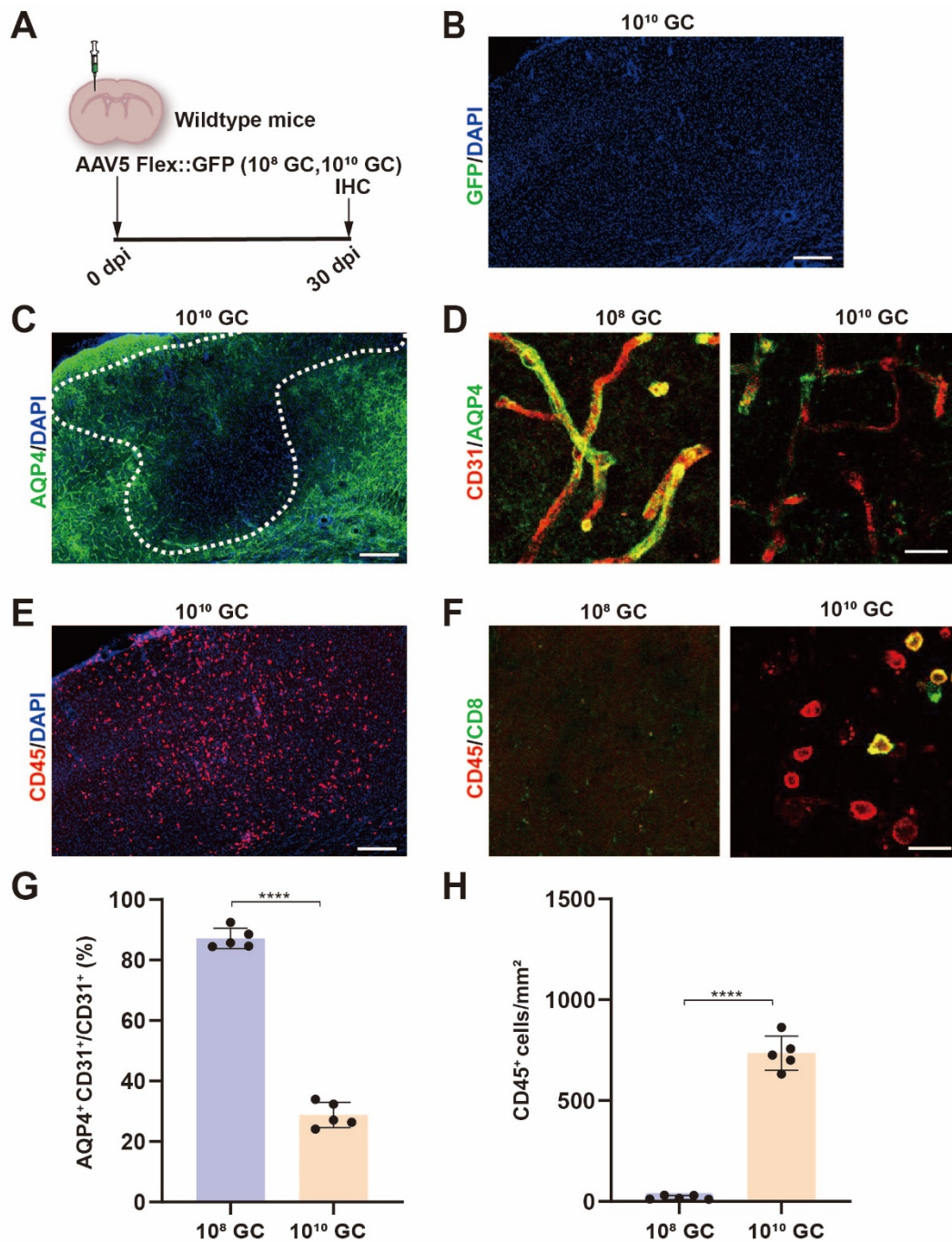


**Figure S7. High-titer AAV5 induced BBB breakdown and leukocyte infiltration also independent of GFP expression.** (A) Experimental design. AAV5-CAG::Flex-GFP was injected in wild-type mouse cortex. (B) No GFP expression in wild-type mouse brain after injection of AAV5-CAG::Flex-GFP. Scale bar = 200  $\mu$ m. (C) AQP4 signals were lost at the site of AAV5 injected area (white dashed box). Scale bar = 200  $\mu$ m. (D) Confocal imaging of CD31 (red) co-stained with AQP4 (green) in low-titer (left) and high-titer AAV5 (right) treated mice at 30 dpi. Scale bar = 20  $\mu$ m. (E) CD45 positive leukocytes were invaded into the mouse brain parenchyma after high-titer AAV5 injection. Scale bar = 200  $\mu$ m. (F) Confocal imaging of CD45 (red) co-stained with CD8 (green) in low-titer (left) and high-titer AAV5 (right) treated mice at 30 dpi.

Scale bar = 20  $\mu\text{m}$ . (G) Quantification data showing that perivascular astrocytic endfeet were significantly reduced after injection of high-titer AAV5 at 30 dpi. (H) Quantitative data showing significant leukocyte invasion in high-titer AAV5 treated group. Values are shown as mean  $\pm$  SD. n = 5 mice per group. Two-tailed Student's t-test. Significance reported as \*\*\*p < 0.0001.

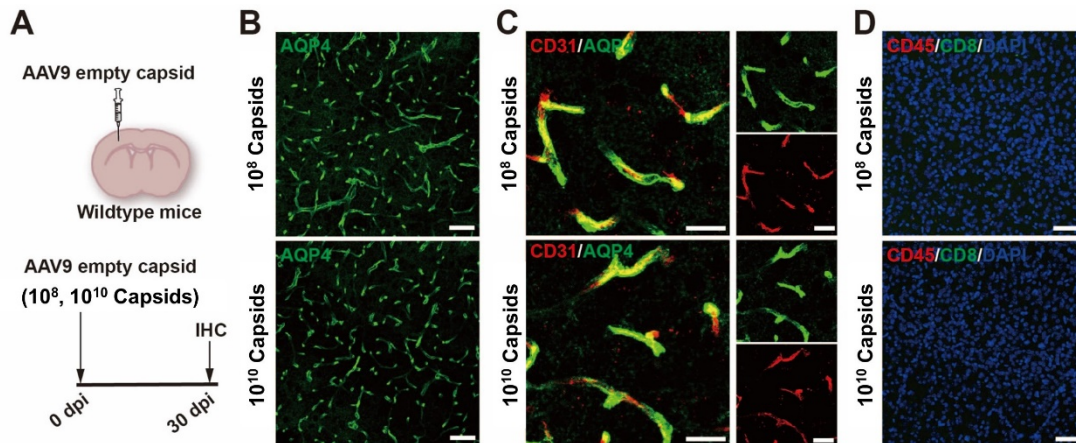


**Figure S8. Injection of empty AAV9 viral capsids did not induce BBB disruption and leukocyte invasion in brain parenchyma.** (A) Experimental design. (B) Low magnification confocal images of immunostaining for the astrocytic endfoot marker AQP4 surrounding the injection site of empty viral capsid. Note that neither low titer (top) nor high titer (bottom) empty capsids caused any apparent loss of AQP4 signal (n = 5 mice per group). Scale bar = 50  $\mu\text{m}$ . (C) High magnification confocal images of CD31 (red) and AQP4 (green) co-immunostaining. The fluorescent signal of CD31 is perfectly encapsulated by AQP4, which is observed in both low-titer (top) and high-titer (bottom) empty viral capsid treated mice. Scale bar = 20  $\mu\text{m}$ . (D) Leukocyte infiltration was not detected after AAV9 empty capsid injection (n = 5 mice per group). Scale bar = 50  $\mu\text{m}$ .

**Table S1. AAV information**

<b>Virus</b>	<b>Promoter and length</b>	<b>Volume</b>	<b>Original titer</b>
AAV9 GFAP2.2::GFP	GFAP2.2 (2210 bp)	0.1-1 $\mu$ L	$2.30 \times 10^{13}$ GC/mL
AAV9 GFAP1.6::GFP	GFAP1.6 (1677 bp)	1 $\mu$ L	$7.70 \times 10^{13}$ GC/mL
AAV5 GFAP2.2::GFP	GFAP2.2 (2210 bp)	1 $\mu$ L	$2.50 \times 10^{13}$ GC/mL
AAV5 GFAP681::GFP	GFAP681 (681 bp)	1 $\mu$ L	$3.47 \times 10^{13}$ GC/mL
AAV9 FLEX::GFP	CAG (868 bp)	1 $\mu$ L	$6.09 \times 10^{13}$ GC/mL
AAV5 FLEX::GFP	CAG (868 bp)	1 $\mu$ L	$8.34 \times 10^{13}$ GC/mL
AAV9 empty capsid	None	1 $\mu$ L	$1.56 \times 10^{14}$ Capsids/mL

**Table S2. Primary antibody information**

<b>Antibodies(dilution)</b>	<b>Host</b>	<b>Source</b>	<b>Catalog#</b>
AQP4 (1:1000)	Rabbit	Proteintech	16473-1-AP
CD31 (1:300)	Rat	BD Bioscience	550274
CD45 (1:500)	Rat	BD Bioscience	550539
CD45 (1:500)	Rabbit	Cell Signaling	70257
CD4 (1:500)	Rat	ThermoFisher	14-0042-82
CD68 (1:1000)	Rabbit	Abcam	Ab125212
CD8 $\alpha$ (1:1000)	Rabbit	Abcam	Ab217334
GFAP (1:1000)	Rat	Invitrogen	13-0300
GFAP (1:1000)	Rabbit	DAKO	Z0334
Iba1 (1:1000)	Rabbit	Wako	019-19741
ZO-1 (1:300)	Rat	DSHB	R26.4C
Occludin (1:300)	Mouse	Santa Cruz Biotechnology	sc-133256
CD41 (1:1000)	Rat	Abcam	Ab33661
CD31 (1:300)	Rabbit	Abcam	Ab28364
CD19 (1:500)	Mouse	Santa Cruz Biotechnology	sc-373897
NeuN (1:2000)	Guinea pig	Millipore	ABN90
GFP (1:2000)	Chicken	Abcam	Ab13970
Granzyme B (1:2000)	Mouse	Santa Cruz Biotechnology	sc-8022